Analysis of Conformational Polymorphism in Pharmaceutical Solids Using Solid-State NMR and Electronic Structure Calculations

Jay R. Smith,[†] Weizong Xu,[‡] and Daniel Raftery*

Department of Chemistry, Purdue University, 560 Oval Drive, West Lafayette, Indiana 47907

Received: October 27, 2005; In Final Form: February 28, 2006

A detailed analysis of molecular structure in three polymorphic forms of 5-methyl-2-[(2-nitrophenyl)amino]-3-thiophenecarbonitrile is made using a combination of multidimensional solid-state NMR (SSNMR) experiments and molecular modeling via electronic structure calculations. These compounds, collectively referred to as ROY because of their red, orange, and yellow colors, share a similar molecular structure with the exception of the dihedral angle between the phenyl and thiophene rings. The ROY materials make it possible to study the influence of nearly a single degree of freedom on the associated NMR spectra. Using the 2D PASS (Antzutkin et al. *J. Magn. Reson. A* **1995**, *115*, 7) experiment, spectral editing techniques, and DFT-based calculations of the local fields, an analysis is made of the sensitivity of all carbon and nitrogen sites to changing molecular conformation. Chemical shift and dipolar coupling information obtained from these experiments vary noticeably between forms and are subsequently used to quantitatively determine aspects of molecular structure in these materials, including the coplanar angle between the phenyl and thiophene rings. The influence of motion on the methyl and nitro chemical shifts is also investigated. The accuracy of the information obtained from local field analysis and the model structure calculation demonstrates the capabilities of SSNMR as a quantitative structural method.

Introduction

Polymorphic solids share the same chemical composition but exhibit a variety of different crystal structures due to molecular flexibility and changing crystallization conditions.[1] Polymorphism plays an important role in the development of new pharmaceutical solids, since the structural differences often have a significant effect on their physicochemical properties, such as stability, dissolution rates, bioavailability, and proccessability.[1,2] An important subclass of polymorphism is conformational polymorphism, where a molecule can adopt different conformations through a controlled crystallization process. Since conformational differences can result in variations in internuclear distances and local electronic structure, solid-state nuclear magnetic resonance (SSNMR) is an ideal and sensitive probe for characterizing this type of behavior and can provide complementary information to other structural analysis techniques. In some cases, SSNMR has accurately yielded evidence of polymorphism when X-ray methods falsely indicated the presence of only a single structure.[3]

Anisotropic interactions measured by SSNMR contain information on local molecular structure. Through both molecular structure and electronic contributions, conformational differences between polymorphs can manifest themselves as variations in the local field information evident in the SSNMR spectra. Extracting this information from measured tensor values can be difficult due to the complexity of the problem, but the process can be facilitated with the aid of theoretical calculations. This methodology has gained renewed interest in part because it can be aided by the concurrent use of ab initio methods. The combination of measured and predicted chemical shift anisotropy (CSA) tensor values has been used to determine aspects of local structure in a variety of chemical systems, including bond lengths and dihedral angles in protein and peptide backbones,[4,5] binding orientations of CO ligands to heme proteins,[6] and structural differences in various forms of diamond.[7]

Although this methodology can be readily applied to pharmaceutical solids, only a handful of SSNMR studies (nearly all involving 1D techniques) have used tensor information to investigate structural issues in polymorphic compounds. For example, ^{13}C CSA tensor analysis has been used to deduce hydrogen bonding patterns,[8] to reveal local conformational and motional changes through specific functional groups, and to correlate directly with crystallographic information.[9] Analysis of ^{15}N spectra has shown that nitrogen CSA tensor values can also change significantly with changes in crystal morphology.[10]

In molecular systems with only a few distinct chemical sites, or compounds that have been selectively labeled, 1D SSNMR techniques are often sufficient for resolving the desired spectral features. However, even in moderately complex organic solids, the overlapping spectral features and high density of spinning sidebands make analysis much more challenging. Multidimensional SSNMR experiments can facilitate local field analysis by spreading the spectral information over several dimensions. Among the numerous methods available, 2D experiments that separate isotropic from anisotropic tensor information along separate frequency axes are extremely powerful. A variety of chemical shift separation techniques have been developed over the years, ranging from multiple pulse sequences to mechanical manipulations of the sample.[11−21] Two of the more successful approaches include 2D PASS[20] (based on the original Phase Altered Separation of Sidebands experiments by Dixon[11]) and FIREMAT (FIve π REplication Magic Angle Turning).[21,22] Both of these 2D experiments have recently been applied to organic

* To whom correspondence should be addressed. E-mail: raftery@purdue.edu.
† Present address: CNA Corporation, Alexandria, VA.
‡ Present address: Alcoa Technical Center, Alcoa Center, PA.

10.1021/jp056195k CCC: $30.25
Published on Web 03/29/2006

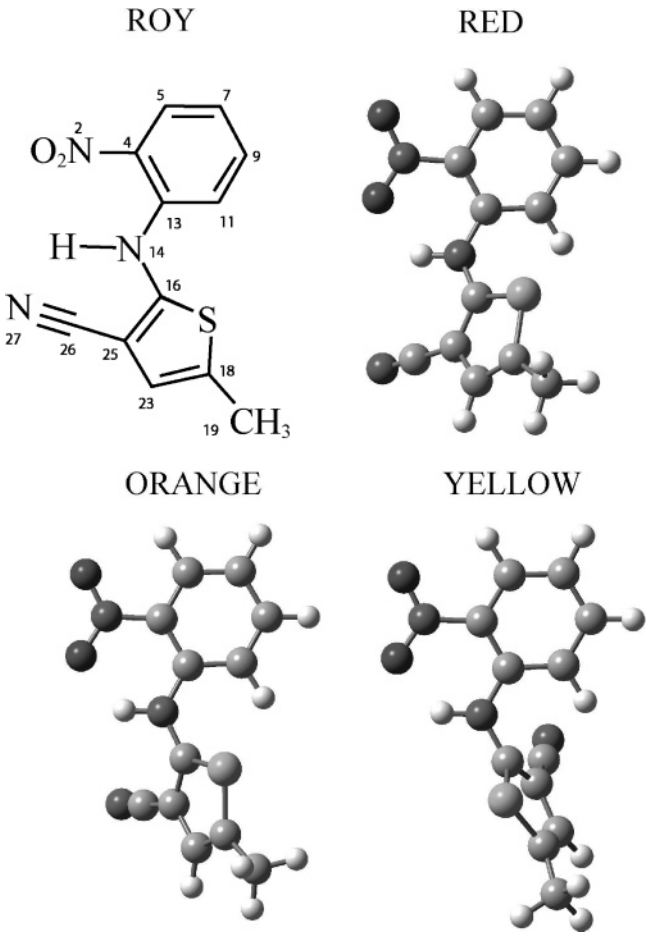

Figure 1. ROY polymorphs. The structures were provided from previous studies of these materials and were deduced using X-ray techniques.[29] The input numbering scheme used in all electronic structure calculations is shown along with the chemical structure of the molecule.

and pharmaceutical solids[23,24] Recently, Strohmeier has combined the results of ab initio calculations with 2D SSNMR CSA measurements to obtain a detailed solid-state structure of a tripeptide derivative, melanostatin.[25] More generally, many fine examples of the use of SSNMR to predict structure in solid-state organic molecules have been reported.

Several years ago, we and others demonstrated the utility of combining 2D SSNMR anisotropic/isotropic separation experiments with ab initio calculations for structural studies of conformational polymorphism.[26−28] In the present study, we have applied the 2D PASS chemical shift separation experiment along with density functional theory (DFT) calculations to analyze the structural information available in the SSNMR spectra of a polymorphic organic solid. The molecular system chosen includes three of the seven known crystalline polymorphic forms of 5-methyl-2-[(2-nitrophenyl)amino]-3-thiophenecarbonitrile[29] (illustrated in Figure 1), which are known collectively as ROY due to their red, orange, and yellow colors. In addition to analyzing the ^{13}C chemical shift tensors for each of the 12 carbon atoms in the molecule, we have measured a variety of structural information pertaining to the nitrogen sites. Indirect information encoded in the ^{13}C line shapes due to through-space couplings yields information on the dipolar and electric field gradient tensors associated with neighboring ^{14}N nuclei. 1D ^{15}N CPMAS (cross-polarization magic angle spinning) spectra were also acquired for each of the ROY forms to analyze the nitrogen CSA tensors. The information extracted from the carbon and nitrogen NMR experiments, in conjunction with density functional calculations, is used to investigate the variations in the local fields between forms and to assign an origin to these variations in terms of molecular conformation. We discuss the relative sensitivities of some sites to the local geometrical changes and suggest a possible explanation for this phenomenon based on intramolecular charge transfer. To probe the relationship between chemical shift and local molecular structure further, chemical shielding calculations were performed on model structures based on the major conformational difference in the ROY forms, namely, the phenyl−thiophene coplanar angle. From this information, we were able to quantitatively determine the coplanar angle for each ROY form in the absence of any other structural information by comparing measured tensor values to calculated shieldings. The results of our work illustrate the power and potential of SSNMR and electronic structure calculations for quantitatively determining molecular structure in pharmaceutical polymorphs and, by extension, a variety of other materials.

Experimental Section

The polymorphic forms of ROY were gifts from Eli Lilly and Company and had ^{13}C (1%) and ^{15}N (0.3%) in natural abundance. All spectra were recorded on a commercial Varian Unity Plus spectrometer at room-temperature operating at a ^{1}H resonance frequency of 300 MHz and using a Chemagnetics 5 mm PENCIL probe. The ROY compounds had ^{1}H T_1 times ranging from 20 to 50 s such that CPMAS recycle delays of 25−65 s were necessary for optimal signal averaging. To shorten the effective ^{1}H T_1, all CP experiments included an additional ^{1}H flip-back pulse after acquisition. The optimal recycle delay was then observed to be 3−10 s.

Each ^{13}C 2D PASS experiment used a total of 16 t_1 increments and thus covered sideband orders from +8 to −8. The MAS rate was fixed at 1600 Hz resulting in a spectral width of 24 kHz in ω_1 and a pitch spacing between increments of 22.5°. The pulse timings were calculated using the PASS equations and are shown and tabulated in Supporting Information Figure S1 and Table S2. A ^{13}C B_1 field strength of 86 kHz was employed, and pulse imperfections were compensated using a 243-step pulse phase cycle involving independently stepping each π-pulse through 3 phases of 0°, 120°, and 240°. The total number of signal transients acquired (typically 1215) was chosen to be a multiple of 243, with the total acquisition time being approximately 48 h. The spectra were externally referenced to a labeled glycine sample, with the methylene ^{13}C resonance set to 43.4 ppm.

The two ^{13}C spectral editing experiments used in our analysis are depicted in parts b and c of Figure 2 and were performed at a spinning speed of 6 kHz. The first experiment, shown in Figure 2b, uses a short contact pulse (CP, 140 μs) and yields signal for sites with one or two attached protons. Only sites that are strongly coupled to protons can build up an appreciable amount of signal during such a short contact period. The second experiment, Figure 2c, is designed to nullify the signal from sites with one and two attached protons, leaving only unprotonated and methyl resonances. The sequence begins with a long contact period (8 ms) designed to excite all carbon sites, but then the signal from the strongly coupled sites is eliminated by an appropriate inversion period (140 μs). The spectral editing pulse timings were optimized on a methionine sample, which has all four types of carbon protonation.

An ^{15}N CPMAS spectrum was obtained for each of the ROY forms. A CP contact time of 8 ms was used for each sample but was not optimized due to the poor sensitivity of the ^{15}N

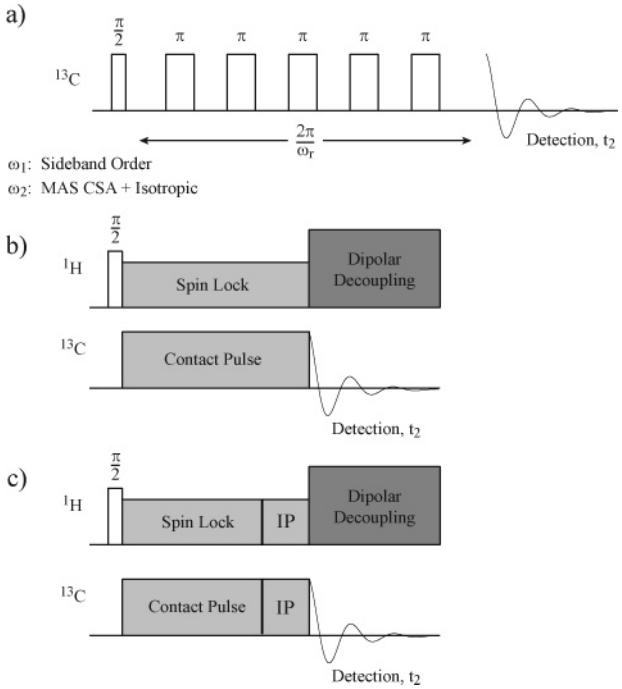

Figure 2. (a) Pulse sequence used for the 2D PASS experiment. The preparation period is depicted as a single 90° pulse but can be replaced with cross-polarization. The pulse timings are calculated by solving the PASS equations and are illustrated and tabulated in Supporting Information Figure S1 and Table S2. (b) Spectral editing pulse designed to excite only sites with strong proton couplings such as R−^{13}CH−R′ and R−^{13}CH$_2$−R′ using a short CP period. (c) Spectral editing sequence that eliminates R−^{13}CH−R′ and R−^{13}CH$_2$−R′ resonances using a long, nonselective CP period followed by a properly timed inversion period that negates the signal from these sites leaving only R−^{13}C−R′ and R−^{13}CH$_3$ carbon signals.

spectra. The MAS rate chosen for each experiment was made based on theoretically determined CSA tensor values and ranged from 1.2−1.4 kHz. To achieve a sufficient signal-to-noise ratio, the spectra were recorded over a period of 3−5 days recording a total of 10 000−100 000 signal transients. The spectra were externally referenced to a labeled glycine sample, with the amine resonance set arbitrarily to zero.

Local field information pertaining to ^{13}C and ^{15}N sites was extracted from the MAS powder patterns using a line shape fitting process that closely follows the procedure outlined by de Groot et al.[30] and by Suits[31] for the case of residual dipolar couplings to quadrupolar nuclei. Tensor values were extracted from the experimental line shapes using an interactive C/C++ fitting program and the analysis was performed on a desktop PC. The Alderman octahedral tiling scheme was used to pick 264 uniformly distributed points on this unit hemisphere, which facilitated the use of the three-point, triangular interpolation.[32] A Simplex routine[33] was used to adjust the fitted tensor values until the numerically calculated sideband intensities agreed well with experimental values. Error values were calculated using uncorrelated, parabolic error analysis. A total of 15 parameters was needed to fit the ^{13}C line shapes split by coupling to neighboring ^{14}N sites (4 broadening parameters, 3 chemical shift parameters, 3 dipolar tensor parameters, and 5 electric field gradient tensor parameters), requiring approximately 6 s of computation per iteration on a 1.2 GHz Athlon processor-based PC. The line shapes for uncoupled sites required a total of 9 free parameters and took significantly less computation time per iteration, approximately 1 s. Convergence in the fitting analysis was typically achieved between 100 and 1000 iterations.

Theoretical calculations were performed on a desktop 400 MHz Pentium II-based PC and an IBM RS-6000 computer cluster using the Gaussian 98 program.[34] All calculations used a density functional approach with the hybrid B3LYP functional[35,36] and a 6-311G Gaussian basis set.[37,38] The proton positions in the X-ray structures were adjusted by energy minimization while holding all other degrees of freedom constant. The rotational calculations used in the investigation of motional averaging were made using the proton-relaxed ROY X-ray structures[29] as input coordinates and incrementing an appropriate dihedral angle in 10° steps (the H20−C19−C18−S17 and the C05−C04−N02−O01 dihedral angles for the methyl and nitro groups, respectively). The initial structure in the molecular modeling of the phenyl−thiophene coplanar angle was determined by performing a complete energy minimization on the ROY compound. The C11−C13−C16−S17 dihedral angle was used to approximate the phenyl−thiophene coplanar angle. A total of 72 increments were used in the rotation with a step size of 5°. At each step, the dihedral angle was fixed and the remainder of the ROY structure was allowed to relax by energy minimization. After minimization was complete, an NMR shielding calculation was performed using gauge-including atomic orbitals[39] and the true coplanar angle was determined by the scalar product of the phenyl and thiophene plane-normal vectors. The geometry optimization for the last two steps in the rotation did not converge.

Results and Discussion

Spectral Assignments. A 2D PASS spectrum for ROY-red is shown in Figure 3. The data have been sheered to align all of the resonances in the spinning sideband manifold for a given isotropic resonance to a single frequency in ω_2. Shown to the right of the contours are traces taken at the distinct atomic sites, which illustrate the spinning sideband manifolds that vary in breadth from 50 to 350 ppm. To proceed further with line shape analysis, it is necessary to make an unambiguous assignment of the isotropic resonances to specific molecular sites. Our approach begins with the use of spectral editing experiments to characterize the protonation of all of the carbon resonances. Then, unusually broad or split peaks are flagged as belonging to sites directly bonded to neighboring nitrogen atoms. Finally, the measured tensor values extracted from line shape analysis for each site category are assigned to a unique site by a least-squares comparison to chemical shieldings derived from DFT calculations. The only assumptions necessary for applying this assignment scheme are (1) all sites must exhibit some difference in isotropic positions or line widths beyond the spectral resolution and (2) ambiguous sites resolved by least-squares comparison to theory must be distinguishable beyond the nominal discrepancy between theory and experiment (in this study, 3−8 ppm).

The results of the spectral editing experiments designed to differentiate nonprotonated and single protonated carbon sites are illustrated for each of the ROY compounds in Figure 4. The methyl carbons are not shown but have already been identified at shifts of 16−18 ppm. As expected for these compounds, the spectra for the nonprotonated and single-protonated carbons have a total of six (C04, C13, C16, C18, C25, and C26) and five resonances (C05, C07, C09, C11, and C23), respectively. At first glance, it may appear that there are only five nonprotonated resonances but the nitrile site (identified below to have isotropic shifts of red = 116.1 ppm, orange = 114.3 ppm, yellow = 115.2 ppm) has an extremely large CSA and a relatively small isotropic peak at these spinning speeds.

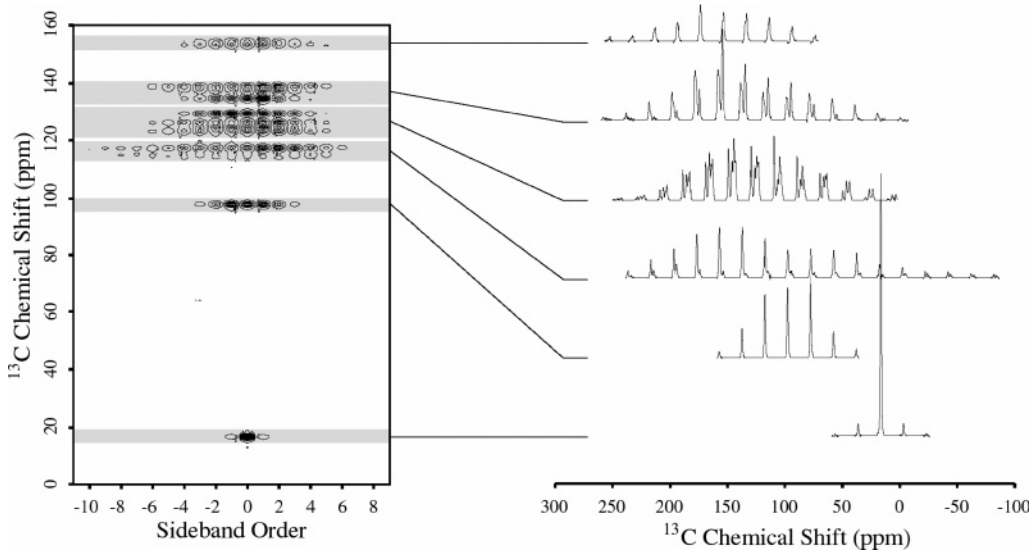

Figure 3. Contour plot of the 2D PASS spectrum for ROY-R. Included to the right of the spectrum are isotropic slices showing the spinning sideband manifold for each site.

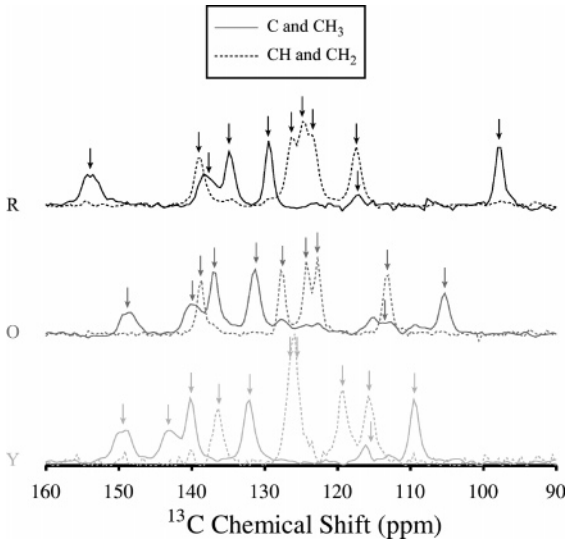

Figure 4. Spectral editing experiments for all three ROY forms. The spinning speed was 6 kHz so no sidebands are present in these spectra.

Three resonances in each spectrum show pronounced splitting and correspond to the nitrile (C26) and two amine carbons (C13, C16). The nitro carbon resonances (C04) are predicted by theory to have only slight splittings, on the order of the intrinsic line widths (~90 Hz).

To resolve ambiguities in the assignment process, we use the results of DFT chemical shielding calculations for each of these carbon sites. In some situations, the agreement between theory and experiment is sufficient to allow for the unambiguous assignment of the isotropic spectrum. However, closely spaced or overlapping resonances are difficult to assign reliably using this isotropic identification method. The discrimination process can be greatly refined by the use of all three principal tensor values. This point is illustrated in Figure 5 for three isotropic resonances separated by less than 1 ppm. Despite the similarity in the isotropic values, the breadth and symmetry of the CSA tensors vary greatly between these sites, making them more distinguishable. In some cases, sites determined to have the best agreement between theory and experiment for all three principal values will not be closest in isotropic frequency. The easiest method of incorporating the calculated shielding information

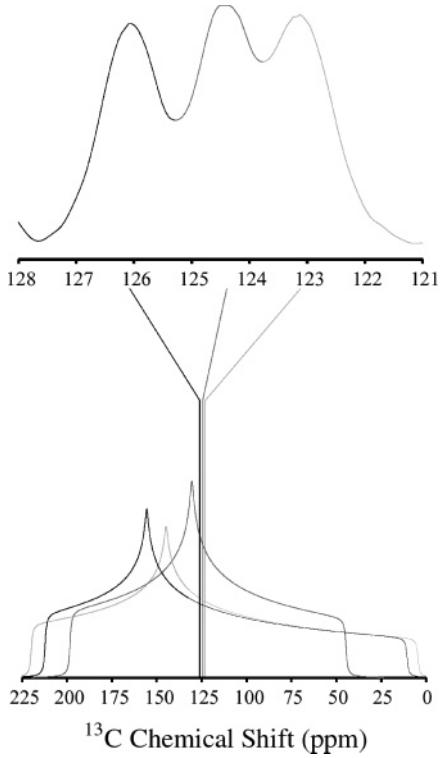

Figure 5. Three ^{13}C resonances in ROY-R that share similar isotropic shifts but have large variations in the asymmetries and anisotropies of the chemical shift tensors. The static patterns were calculated from the CSA principal values obtained from line shape analysis of the 2D PASS data. Notice the differences in scales between the spectrum at the top and spectra at the bottom.

into the assignment process is to make least-squares comparisons of the CSA tensor. In this approach, the site with the calculated tensor values that give the smallest square difference to the measured principal values is the most appropriate assignment. This information can be combined with the peak splittings and the spectral editing data discussed above in an assignment scheme that has four identifying characteristics in the classification: (1) number of attached protons, (2) isotropic chemical shift region, (3) presence of an attached nitrogen atom, and (4) least-squares fit to theoretical tensor values obtained using DFT. Assignment of the ^{15}N CPMAS spectra was considerably easier

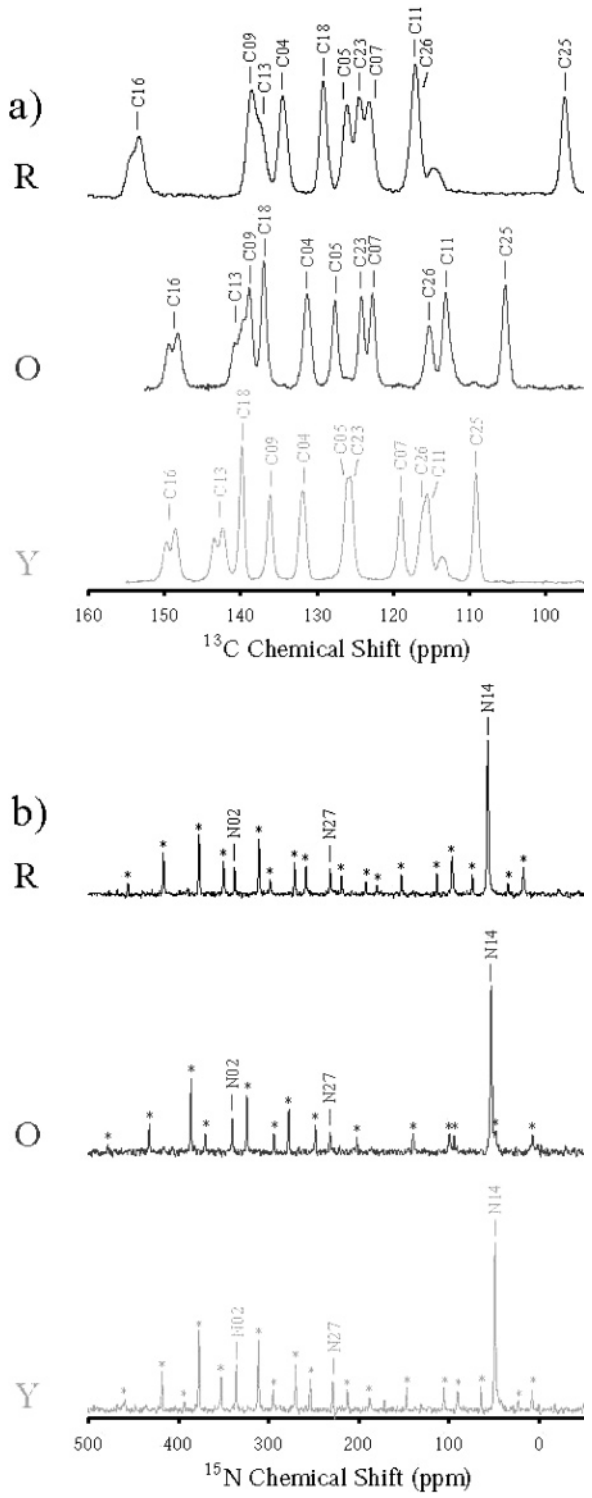

Figure 6. Assignments of the (a) carbon (isotropic only) and (b) nitrogen spectra for the ROY compounds. The numbering scheme used to label the sites is shown in Figure 1. The asterisks denote spinning sidebands.

to make due to the small number of resonances and the relatively large isotropic spacings.

The complete assignments for each ROY compound using this method are shown in Figure 6 for all three ROY compounds. Some interesting results from the assignments are the apparent coincidences in the isotropic resonances between forms. For example, the red and orange forms have two resonances at about 131 and 137 ppm. In the red form, the assignments correspond to C04 (131.8 ppm) and C18 (138.5 ppm), but in the orange form, the assignment is the reverse C04 (136.7 ppm) and C18 (130.3 ppm). Changing peak assignments to keep the order of the C04 and C18 sites the same between red and orange forms would raise the root mean square (rms) difference in tensors values for the forms from ~3 to ~26 ppm. Several of the resonances in each spectrum are only distinguishable by use of the full CSA tensor. The yellow form, for instance, has two resonances separated by less than 1 ppm, namely, the C04 (131.4 ppm) and C09 (132.4 ppm). In isotropic frequency, these sites are nearly identical, but the breadths of the CSA tensors make them easily distinguishable (110.1 ppm for C04 vs 228.0 ppm for C09). These results underscore the unreliability involved in making assignments based on comparison to liquid-state spectra due to the extreme sensitivity of some chemical shifts to molecular structure.

Using all of the tensor values for each form, we have derived the following linear relationships between bare nucleus values and chemical shifts for the carbon and nitrogen sites

carbon:

$$\delta_{\text{shift}} = -0.948\sigma_{\text{shielding}} + 176.7 \text{ ppm}$$

nitrogen:

$$\delta_{\text{shift}} = -0.950\sigma_{\text{shielding}} + 195.8 \text{ ppm} \quad (1)$$

with rms deviations of 6.9 and 13.5 ppm, respectively. These rms values are a measure of the statistical reliability of the calculated shieldings. The correlations between theory and experiment are displayed graphically in Supporting Information Figure S3. The intercepts in eq 1 represent the values for the bare nuclei of the reference materials, namely, TMS and glycine, and the linearity is determined by a combination of the level of theory in the calculations and the quality of the input structure (how well this single molecular structure represents the crystallites in the solid state). A significant contribution to the deviation between theory and experiment can be attributed to intermolecular effects in the crystal packing. Theoretical calculations on single molecules are inherently more similar to the gas phase than to solid-state configurations. The incorporation of neighboring molecules into carbon shielding calculations has been shown to improve the correlation between theory and experiment by as much as 2−3 ppm in some cases.[40] Regarding the nitrogen CSA deviations, it has been shown that nitrogen chemical shifts are particularly sensitive to partial charges in the lattice.[41] This could significantly improve the results for ROY-Y, which is known to exhibit intermolecular hydrogen bonding between the nitrile and amine groups of neighboring molecules.[42]

Molecular Structure from Residual ^{13}C−^{14}N Dipolar Couplings. In the presence of a quadrupolar nucleus, such as ^{14}N, the dipolar Hamiltonian cannot be truncated with respect to the quadrupolar spin, due to its perturbation on the ^{13}C Zeeman states. The effects of these residual couplings on the MAS manifold are manifested as distortions in the line shapes of the spinning sidebands, as evident in the C13, C16, and C26 resonances in Figure 6a. Integration over the spinning sidebands results in a split line shape with a peak ratio of 2:1 due to the populations of the ^{14}N spin states $(P_{+1} + P_{-1}):P_0$. The origin of this 2:1 splitting is well-known and has been discussed in the literature.[43,44] It derives from the fact that the nitrogen quadrupole interaction is nearly the same order as the Zeeman energy, and thus, truncation of the quadrupole term is not complete. Nonsecular terms result and give rise to the observed splitting and distortions seen in the MAS spectra. Importantly,

TABLE 1: Measured and Calculated ^{13}C and ^{15}N Local Field Tensors for ROY-red[a]

site source	δ_{iso} (ppm)	δ_{xx} (ppm)	δ_{yy} (ppm)	δ_{zz} (ppm)
C04 exp	134.4 ± 0.1	186.6 ± 3.7	150.5 ± 4.7	66.2 ± 2.8
calcd	136.9	183.9	157.2	69.5
C05 exp	126.1 ± 0.0	212.1 ± 6.6	155.5 ± 10.1	10.6 ± 7.6
calcd	128.7	220.2	151.3	14.5
C07 exp	123.0 ± 0.1	219.8 ± 6.2	144.7 ± 10.0	4.6 ± 7.8
calcd	118.8	213.1	131.8	11.5
C09 exp	138.8 ± 0.1	248.0 ± 9.2	163.4 ± 13.7	4.8 ± 10.1
calcd	134.6	241.9	148.1	13.7
C11 exp	117.1 ± 0.1	196.8 ± 5.0	136.0 ± 7.8	18.6 ± 5.9
calcd	117.4	204.9	134.0	13.2
C13 exp	137.7 ± 0.1	211.3 ± 4.9	164.6 ± 7.1	37.2 ± 5.1
calcd	139.5	202.8	172.9	42.8
C16 exp	153.6 ± 0.1	228.2 ± 3.7	157.8 ± 5.2	75.0 ± 3.5
calcd	155.5	231.5	157.6	77.5
C18 exp	129.1 ± 0.0	52.0 ± 3.4	123.8 ± 4.9	211.4 ± 3.6
calcd	130.5	58.1	122.1	211.3
C19 exp	16.4 ± 0.0	25.1 ± 5.9	24.2 ± 6.0	0.0 ± 1.0
calcd	18.6	32.4	26.5	−3.1
C23 exp	124.4 ± 0.0	198.2 ± 3.9	130.4 ± 5.5	44.6 ± 3.9
calcd	123.8	196.5	123.2	51.7
C25 exp	97.4 ± 0.0	44.4 ± 1.3	92.1 ± 1.8	155.8 ± 1.2
calcd	98.7	51.8	94.6	149.7
C26 exp	116.1 ± 0.2	228.4 ± 21.0	202.8 ± 24.6	−82.7 ± 12.9
calcd	112.7	218.9	216.1	−97.0
N02 exp	337.6 ± 0.1	456.6 ±12.7	395.7 ± 15.9	160.5 ± 9.6
calcd	331.7	454.7	384.9	155.6
N14 exp	59.6 ± 0.1	97.1 ± 12.3	80.5 ± 12.6	−6.9 ± 2.6
calcd	63.8	109.3	84.8	−2.7
N27 exp	231.6 ± 0.0	388.0 ± 6.0	317.6 ± 7.7	10.8 ± 4.8
calcd	239.7	399.2	335.5	−15.8

[a] Calculated tensor values are based on X-ray derived input structures.

these splittings give important information on the size and relative orientation of the electric field gradient and dipolar couplings. Each ROY compound has a total of four carbon sites that can possibly be split by coupling to a neighboring ^{14}N nucleus, namely, the nitro, amine, and nitrile carbons.

With the isotropic resonances identified, it is possible to investigate the structural information encoded in the dipolar splittings. These couplings provide direct information on molecular structure through the dependences of the dipolar tensors on the $^{13}C-^{14}N$ internuclear vectors and indirect information through the EFGs and relative tensor orientations. The measured coupling parameters as well as those predicted by theory are summarized for all three ROY compounds in Tables 1 and 2, as well as in Supporting Information Tables S4 and S5. The agreement between experiment and theory is quite good but is somewhat artificial. Not all of the dipolar and electric field gradient (EFG) parameters can be measured independently. For example, the dipolar coupling strength and the EFG anisotropy are always present as a product and therefore cannot be distinguished. However, it is appropriate to say that the experimental results are consistent with the theoretical parameters.

Unfortunately, the parameters determined from these splittings have associated error values larger than the variations observed between ROY forms due to the lack of resolution necessary for making precise measurements of these effects. However, some general observations can be made concerning the distinct nitrogen environments in the ROY compounds as a whole. The largest splittings are found for the C26 nitrile carbons, which have moderate nitrogen EFG anisotropies (approx. −3.5 MHz) and the shortest carbon−nitrogen bond lengths (∼1.14 Å). Although these sites have appreciable splittings, the resonances are masked by overlap with the C11 resonance, making them difficult to distinguish. The nitrile carbons also suffer from unusually large CSAs (∼310 ppm in span), decreasing the relative sensitivity of the individual sidebands in the MAS manifolds and hiding the resonances under the C11 sidebands. The C16 amine carbons show the most pronounced couplings, partially because of their isolation in the ^{13}C spectrum. The amine carbons have bond lengths that are much longer than the nitrile carbons (∼1.38 Å), but the corresponding EFG anisotropies are slightly larger (approx. −3.8 MHz). The C13 amine sites show roughly the same sized couplings as the C16 sites but are somewhat obscured by overlap with the C09 resonances. The C13 and C16 carbons are coupled to the same nitrogen sites and should in principle produce the same EFG tensors. The C04 carbon sites, directly bonded to the nitro groups, show no appreciable splitting. However, the line widths of these resonances (∼91 Hz) are somewhat larger than the nominal carbon line widths (∼81 Hz) and can provide an upper bound on the coupling strength between the ^{13}C and ^{14}N.

The EFG and dipolar tensor information contained in the split carbon line shapes includes the relative orientations of the dipolar, EFG tensors in the CSA PAS (principal axis system). The relative tensor orientations can provide some structural clues when it is known how the tensors of certain sites are oriented in the corresponding molecular segments. This approach involves subjective "hand-waving" and at best provides some qualitative structural information. However, a unique situation arises when several sites are coupled to the same quadrupolar nucleus. It is then possible to get quantitative information on the relative positions of the spin-1/2 sites. For example, the C13 and C16 carbons are both coupled to the N14 amine nitrogen. To get information on the structural relationship between the C13 and C16 sites, consider the orientations of the N14 dipolar and EFG tensors in the C13 and C16 CSA PASs. The dipolar vectors linking the carbons to the amine nitrogen can be expressed in a common frame of reference, namely, the nitrogen EFG PAS, using the relations

$$\vec{V}_D^Q = R(\Omega_Q)\cdot R^{-1}(\Omega_D)\cdot \vec{z} \qquad (2)$$

where $\vec{z}$ is the dipolar vector in the dipolar PAS and $\Omega_D = (\alpha_D,\beta_D,0)$ and $\Omega_Q = (\alpha_Q,\beta_Q,\gamma_Q)$ give the orientations of the

TABLE 2: Measured and Calculated ^{14}N Quadrupolar $\{q_{zz}, \eta_Q, \alpha_Q, \beta_Q, \gamma_Q\}$ and Dipolar $\{D, r_{CN}, \alpha_D, \beta_D\}$ Tensor Information Derived from Spectra of the Four Carbon Sites Coupled to ^{14}N Nuclei for ROY-red

site source (C Site)	q_{zz} (MHz)	η_Q	α_Q (deg)	β_Q (deg)	γ_Q (deg)	D (Hz)	r_{CN} (Å)	α_D (deg)	α_D (deg)
N02 exp	−1.1 ± 0.4	0.4 ± Err[b]	9 ± 49	86 ± 40	86 ± 40	728 ± 246	1.44 ± 0.16	189 ± 49	93 ± 41
(C04) calcd	−0.9	0.3	7	89	89	723	1.45	190	94
N14 exp[a]	−3.4 ± 0.9	0.4 ± 0.7	114 ± 28	156 ± 111	156 ± 111	822 ± 194	1.38 ± 0.11	193 ± 28	88 ± 18
(C13) calcd	−3.5	0.5	115	156	156	828	1.38	193	89
N14 exp[a]	−3.5 ± 0.5	0.6 ± 0.3	46 ± 11	25 ± 57	25 ± 57	824 ± 109	1.38 ± 0.06	157 ± 12	86 ± 11
(C16) calcd	−3.5	0.5	55	19	19	819	1.39	165	85
N27 exp	−3.2 ± 0.4	0.4 ± Err[b]	7 ± 291	183 ± 12	183 ± 12	1484 ± 165	1.14 ± 0.04	252 ± Err[b]	3 ± 9
(C26) calcd	−3.7	0.2	15	180	180	1454	1.15	239	0

[a] N14 is bonded to two carbons. [b] Err indicates the error could not be estimated accurately.

TABLE 3: C13−N14−C16 Bond Angle in the ROY Compounds as Determined from the Relative Orientations of the Dipolar Tensors Using eqs 2 and 3

	$\theta_{C13-N14-C16}$ (deg)	
form	exp	X-ray[a]
ROY-R	124	126
ROY-O	129	126
ROY-Y	134	121

[a] The X-ray values are included for comparison.

dipolar and EFG tensors in the CSA PAS, respectively. With the C13−N14 and C16−N14 dipolar vectors expressed in a common reference frame, the C13−N14−C16 bond angle can be calculated from

$$\theta_{C13-N14-C16} = a\cos\left(\frac{\vec{V}^{Q}_{C13-N14}\cdot\vec{V}^{Q}_{C16-N14}}{|\vec{V}^{Q}_{C13-N14}||\vec{V}^{Q}_{C16-N14}|}\right) \qquad (3)$$

The results for the three ROY compounds are given in Table 3. It is somewhat difficult to associate an error with this bond angle given the complex relationship to measured quantities, but it can be assumed to be relatively large. Nevertheless, the comparison with X-ray results is encouraging.

Motional Averaging of the Interaction Tensors. As in many organic molecules, the ROY compounds contain many aspects of structure that can be subject to motion in the solid state. SSNMR can be a powerful tool for studying certain types of motion that are sufficiently slow as to modulate the local field interactions present in an experiment. However, the time scales for some motions, such as molecular rotations, are much faster and can result in an averaging of the orientational-dependent interactions. In the ROY materials, small functional groups such as the nitro and methyl groups are less likely to be sterically hindered and could potentially rotate freely, averaging the CSA and EFG tensors of the corresponding carbon and nitrogen sites. The measured tensor information in Tables 1, 2, S4, and S5 shows that both the methyl carbon and the nitro nitrogen have near axial CSA symmetries, while the calculated tensors are much more asymmetric. These discrepancies in the symmetry between measured and calculated tensors could be indications of motional averaging. To explore the feasibility for these motions, we calculated the rotational potentials using DFT methods. The potential energy surfaces for (two-well) nitro and (three-well) methyl rotations about their respective axes are shown in Supporting Information Figure S6.

The barrier for free rotation of the nitro group is about 12−14 kcal/mol, depending on the form of ROY. The large magnitude of this potential is due in small part to an intramolecular hydrogen bond between the oxygen atom of the nitro group and the proton of bridging amine nitrogen.[42] Assuming that the free energy accessible to these compounds is roughly the room-temperature thermal energy, $kT \sim 0.6$ kcal/mol, it is easy to see that the nitro group exhibits little to no rotational motion. The situation is different for the methyl group because the rotational barrier is much smaller, having a range of 0.9−1.1 kcal/mol. Methyl groups are well-known for fast, uniaxial spinning around the methyl axis. However, according to the size of this potential, the barrier height is still higher than the accessible thermal energy, limiting the motion of the methyl group to a libration. Librational motions have been found to affect the chemical shifts in temperature-dependent studies by Ramamoorthy and co-workers.[45] This limited free motion is supported by the measured CSA tensors for all three ROY compounds. In each case, the methyl carbon exhibits a nonzero asymmetry in the CSA.

TABLE 4: Effects of Motional Averaging on the Calculated Tensor Values for Free Unaxial Rotation and Thermally Populated Librations

form	source	δ_{iso} (ppm)	δ_{CSA} (ppm)	η_{CSA}
R	exp	16.4 ± 0.0	−16.4 ± 0.0	0.06 ± 0.14
	calcd	18.5	−21.7	0.27
	rotation	18.5	−21.2	0.00
	libration	18.5	−21.5	0.18
O	exp	16.6 ± 0.0	−18.4 ± 0.7	0.07 ± 0.11
	calcd	19.3	−22.0	0.30
	rotation	19.3	−21.5	0.00
	libration	19.3	−21.8	0.20
Y	exp	17.9 ± 0.0	−17.7 ± 0.7	0.06 ± 0.10
	calcd	19.0	−23.0	0.30
	rotation	19.0	−22.2	0.00
	libration	19.0	−22.7	0.20

To account for the effects of the limited methyl rotation, a composite model was made using both librational and free rotational motions populated by Boltzmann statistics

$$P(E) = \frac{e^{-(E/kT)}}{\int e^{-(E/kT)}\,dE} \qquad (4)$$

The model is classical in the sense that it assumes a continuum of thermally accessible states. For the "bound" states or states having energies smaller than the rotational barrier, the librations are assumed to involve simple harmonic motion with classical turning points, $\pm\gamma_0'$, determined by the walls of the potential. The averaging of the chemical shift tensor under this motion is calculated by

$$\langle\sigma\rangle = \int_{-\gamma_0'}^{\gamma_0'} p(\gamma')R^{-1}(\alpha',\beta',\gamma')\sigma R(\alpha',\beta',\gamma')\,d\gamma' \qquad (5)$$

where $p(\gamma') = 1/(\pi\sqrt{\gamma_0'^2-\gamma'^2})$ is the classical probability density[46] for the occupation of the various libration angles, γ'. States with energies larger than the barrier are subject to free uniaxial rotation, and the average tensor is calculated by averaging around the symmetry axis. The results of applying this model to the theoretical tensor values are tabulated in Table 4. Although the averaging model produces theoretical tensors with asymmetries closer to experimental values, there are still significant differences that could result from several sources including experimental errors, population of nonclassical, high-energy rotational states, and lower experimental rotational potential barriers.

Two other motions that could be expected in the ROY compounds are rotations of the phenyl and thiophene rings, however, several factors suggest that these rotations are not energetically feasible. For the phenyl ring, the hydrogen bond between the nitro and amine groups ~0.7 kcal/mol keeps the relative orientation of the ring fixed with respect to the amine proton. The energetics involved in rotating the thiophene ring with respect to the rest of the molecule are discussed in detail below. The potential for this rotation has a double well and barriers of 2−6 kcal/mol. Because the identity of each form appears to be tied to the coplanar angle between rings, it does not seem likely that the thiophene ring exhibits significant motion. Another factor not addressed in this discussion is the steric restrictions imposed by the neighboring molecules in the crystallites.

Chemical Shift Sensitivity to Molecular Structure. From the chemical shift information in Tables 1, 2, S4, and S5, it is

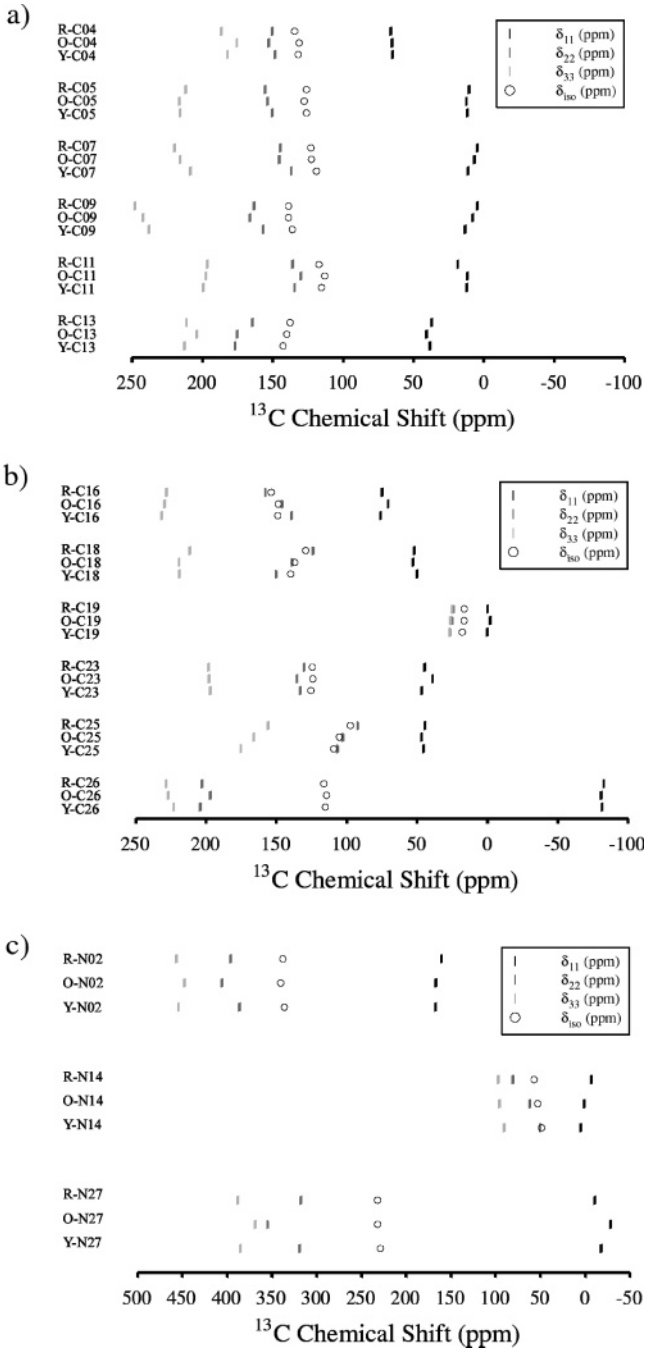

Figure 7. Distribution of ROY tensor values for the (a) phenyl, (b) thiophene, and (c) nitrogen groups. The site numbering scheme is the same as that in Figure 1.

apparent that some sites in the ROY compounds are more sensitive to molecular conformation than others. To aid in the visualization of these conformational dependences, the principal values for all three ROY compounds are plotted graphically in Figure 7 and separated into phenyl, thiophene, and nitrogen sites. Somewhat surprisingly, the chemical shifts for the phenyl carbons do not change dramatically between forms, especially the C04 and C05 sites. The C07 and C09 carbons share similar trends in the breadth of the corresponding CSA tensors, decreasing in magnitude with increasing coplanar angle by 10 and 19 ppm, respectively. An interesting result is that the δ_{xx} and δ_{zz} principal values for these carbons move in concert so as to maintain nearly constant isotropic shifts between forms. As might be expected, the site closest to the thiophene ring rotation (C13), exhibits the largest change in isotropic shift (~5 ppm) but shows no particular trend in the individual principal values. The C11 carbon, α to the C13 carbon, also displays some variation in isotropic shift between forms and in the symmetry of the tensor, while the breadth of the tensor between forms is fairly constant.

In general, the thiophene carbons exhibit larger variations in the CSA tensors than the phenyl carbons. The nitrile and methyl groups are two of the least sensitive sites to the conformational changes. The breadth of the nitrile tensor changes slightly, decreasing by about 5 ppm going from red to yellow, but it is well within the reported error values. Likewise, the methyl isotropic shift varies by roughly 1.5 ppm between forms, but the variation is questionable based on errors associated with the external referencing process (±1 ppm). Another site that shows no appreciable change with morphology is the C23 carbon. The C16 carbon has a unique dependence on conformation, changing primarily in the symmetry of the CSA tensor, while the breadth and the trace of the tensor are relatively unchanged. The two most sensitive positions in the thiophene ring appear to be the C18 and C25 sites. Both of these resonances show pronounced variations in the symmetry and trace of the chemical shift tensor, however, only the C25 carbon exhibits a change in the breadth of the anisotropy (~19 ppm).

The CSA tensors of the nitrogen nuclei in the ROY compounds also show varying conformational changes with structure. All three principal values for the nitro and nitrile sites are nearly identical for the red and yellow forms. The orange form displays some differences in the individual tensor components, but the isotropic shift is very similar to those of red and yellow. The amine nitrogen, which has the smallest CSA, appears to have the greatest chemical shift sensitivity. The symmetry of the tensor is near axial for the red form and becomes almost completely asymmetric for the yellow. The isotropic shift and breadth of the tensor decrease going from the red to the yellow compound by approximately 8 ppm each.

With the phenyl and thiophene rings linked by an amine nitrogen, the ROY compounds are highly conjugated systems. One possible explanation for the diversity in the chemical shift sensitivity exhibited by the carbon and nitrogen sites is based on the extent of intramolecular electron delocalization. In an LCAO-MO (linear combination of atomic orbitals-molecular orbital) sense, the p-orbitals of the atoms in the phenyl and thiophene rings become aligned in the more coplanar polymorphs, which could allow greater transfer of π electrons between the rings. Since the chemical shielding effect is determined by the electronic current density, a transfer of net charge from one molecular segment to another could result in changes in chemical shieldings for both segments. Although this is a severe oversimplification, changes in the overall charge density at each site should give some indication of chemical shift variations between forms.

To determine if this charge-transfer explanation is feasible, the DFT calculations of the Mulliken charge for the three ROY compounds were examined for differences among the functional groups. Surprisingly, little charge transfer is observed between the main functional groups in the ROY molecules. On the basis of the trends going from red to yellow (increasing coplanar angle), it does appear that small amounts of charge are transferred from the nitrile group to the thiophene ring (~0.05 e) and from the phenyl ring to the amine bridge (~0.03 e). However, significant charge transfer can be observed within the individual functional groups. The charge at the C13 site of the phenyl ring shows the same trend as the amine group, increasing from red to yellow, while the C04 and C11 sites, α

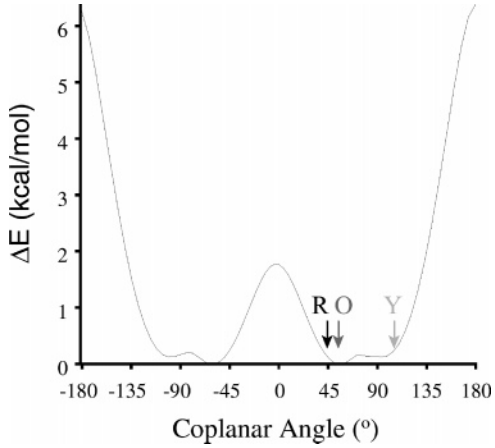

Figure 8. Potential energy surface for thiophene ring rotation in ROY. The angles corresponding to X-ray values are labeled by form.

to C13, behave in an opposite fashion. This is perhaps an indication that the C04 and C11 carbons act as the source of the charge transfer to C13 and N14 sites. The remainder of the phenyl group shows little to no change in charge between forms. The majority of the thiophene group shows little charge dependence on conformation, the major exceptions being the C16 and C25 carbons. The trends in the Mulliken analysis suggest that the rotation of the thiophene group to a more perpendicular coplanar angle causes a transfer of charge (∼0.11 e) from the C25 to the C16 carbon. The effective charges for the atoms in the nitro, methyl, and nitrile groups remain nearly unchanged between forms. These data can be seen graphically in Supporting Information Figure S7.

It appears that charge variations between forms do not necessarily indicate changes in the CSA tensor. For example, the C04 carbon of the phenyl ring exhibits a significant change in effective charge but almost no change in the CSA principal values. On the other hand, the CSAs of the C07 and C09 sites vary by a relatively large amount between forms, yet these sites show little to no change in charge with conformation. One conclusion that can be linked to electron delocalization is that only the sites included in the large conjugation network in the ROY compounds (the phenyl, amine, and thiophene groups) show any significant conformational dependence in the CSA.

Molecular Modeling of the ROY Compounds. The structural relationship between ROY forms is closely linked to the phenyl−thiophene coplanar angle. Even the morphologies of 5-methyl-2-[(2-nitrophenyl)amino]-3-thiophenecarbonitrile excluded from this study are nearly identical, with the exception of this single degree of freedom.[42] To investigate the influence of this parameter on chemical shift tensors, DFT calculations were performed over the entire range of this angle. Unlike the calculations discussed above, the input structure for these calculations was not obtained from X-ray data but rather by complete molecular geometry optimization. Hence, the results in no way rely on a priori knowledge of the molecular structure. A single dihedral angle (C11−C13−C16−S17) was fixed to approximate the relationship between the phenyl and thiophene rings and was stepped through 360° in 5° increments. The remainder of the molecule was allowed to relax at each step by energy minimization prior to calculation of the chemical shieldings.

The potential energy surface due to thiophene ring rotation is shown in Figure 8 and is similar to the one published by Yu et al.[42] The potential has a total of four wells at ±55° and ±90°. Apparently, the molecule is not sensitive to the sign of the rotation, which may be due to its near C_2 symmetry when the phenyl and thiophene rings lie parallel. The highest energy configurations, near 180° ($E_{barrier}$ = 6.2 kcal/mol), are a result of steric effects between the nitrile group and the proton attached to the C11 site (H12). Similarly, the interaction between H12 and the sulfur atom in the thiophene ring (S17) raises the energy of conformations near 0° ($E_{barrier}$ = 1.8 kcal/mol). The conformations of the ROY compounds are also indicated on the potential in Figure 8. The red and orange forms have nearly identical ground-state energies and are located at the minimum of the potential. The yellow form occupies a local minimum separated from the red and orange orientations by a small barrier of ∼0.2 kcal/mol.

The dependences of the carbon and nitrogen chemical shieldings on the phenyl−thiophene coplanar angle are illustrated in Supporting Information Figures S8−S10 by functional group. The shieldings have been converted to shifts using the linear relationships in eq 1. The sites that exhibit the greatest conformational sensitivity are similar to those observed in the ROY forms. Only one of the phenyl carbons shows any significant changes in chemical shift, namely, the C13 site. Strangely, the symmetry and the isotropic position of the C13 CSA change with conformation, but the breadth of the tensor remains fairly constant. The C05, C07, and C09 sites remain unaffected by the conformational changes, and the C04 and C11 sites show only the slightest variations in chemical shifts.

The thiophene ring carbons show more pronounced conformational changes, as evident in Figure S9. C16 displays the most unusual effects, keeping nearly constant isotropic and anisotropic shifts while the asymmetry of the tensor varies dramatically. This could be linked to the change in molecular symmetry at this site upon rotation of the thiophene group. The C18 and C25 sites are by far the most sensitive, with net changes in the breadth of the CSA as large as 50 ppm. The corresponding changes in the isotropic shifts are only as large as 20 ppm, emphasizing the utility of the full tensor in conformational analysis studies using SSNMR. The methyl, nitrile, and C23 sites show little change between orientations. A slight increase in the span of the nitrile carbon CSA is due to the steric interaction with H12 proton of the phenyl ring.

The calculated nitrogen chemical shifts (Figure S10) have a much stronger conformational dependence than those observed in the ROY forms. The maximum changes in breadth and isotropic position of the amine tensor rival those of the C25 carbon at 46 and 28 ppm, respectively. The nitrile nitrogen also shows a much stronger dependence on the thiophene orientation than observed experimentally. As expected, the nitro site is nearly unaffected by the ring rotation.

The apparent discrepancies in the chemical shift sensitivity to conformation between theory and experiment are mostly due to the specific geometries of the ROY forms. The data in Figures 7 and S8−S10 indicate the ROY molecules are located in regions of the rotational potential that are similar in chemical shift. For example, the CSA principal values of C18 show significant movement between ROY forms, but these absolute variances are small relative to the maximum changes observed in the model rotation calculation. Although the calculated and experimental CSA values do not coincide, the calculated results at coplanar angles equivalent to X-ray values show trends very similar to the experimental values, as illustrated in Tables 1, S4, and S5. The somewhat poor absolute agreement between theory and experiment can be attributed to the geometrical degrees of freedom in the ROY molecules that are not accounted

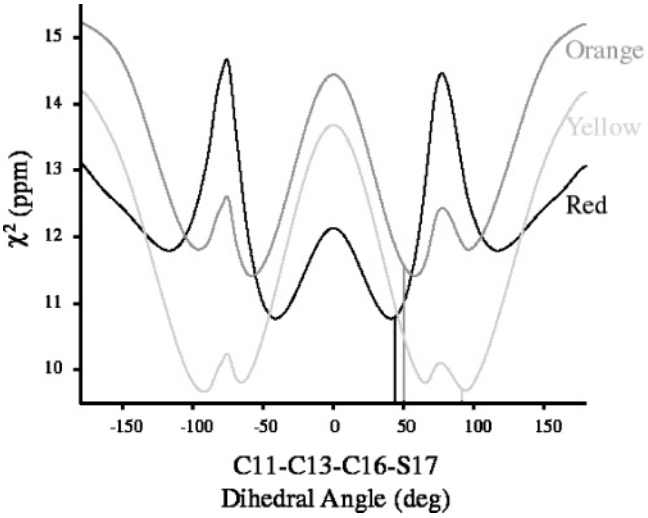

Figure 9. Least-squares comparison of all ^{13}C and ^{15}N tensor values between experiment and molecular modeling. The X-ray values of the C11−C13−C16−S17 dihedral are marked with vertical lines.

for in the model rotation, as well as the presence of neighboring ROY molecules in the lattice structure.

Given the similarity in the trends exhibited by the experimental and model rotation tensor values, it should be possible to use the calculated data to determine the phenyl−thiophene coplanar angle by comparison to measured tensor values. The measured tensor information can be used as molecular constraints in determining the model structure that provides the best correspondence between theory and experiment

$$\chi^2 \equiv \sum_n \left(\sum_{i,j} \left(\frac{A^{(n)}_{\mathrm{exp}_{i,j}} - A^{(n)}_{\mathrm{model}_{i,j}}}{\epsilon^{(n)}_{\mathrm{exp}_{i,j}}} \right)^2 \right) \rightarrow 0 \qquad (6)$$

where $A^{(n)}_{\mathrm{exp}}$ and $A^{(n)}_{\mathrm{model}}$ are the experimental and theoretical local field tensors for the n sites in the ROY molecules, respectively, and $\epsilon^{(n)}_{\mathrm{exp}}$ is the error associated with the experimental tensor. In this study, we only compared CSA tensors, but the comparison need not be limited to chemical shift information and can include the EFG and dipolar tensors determined from the split carbon line shapes. The least-squares functions for all three ROY forms are plotted in Figure 9 as a function of the coplanar angle. As expected, the curves exhibit symmetries about 0° and 180°, but there are also slight symmetries at nearly perpendicular configurations, ±75°. These additional symmetries result in another pair of local minima symmetrically disposed from the true minima about the ±75° mark. The true minima produce slightly better fits to the experimental data (~0.3−1.0 ppm) and the χ^2 statistics at these positions, 9.5−11.5 ppm, are measures of the absolute agreement between the measured and modeled tensor values. Again, correlation between theory and experiment for the model rotation is significantly worse than for the calculations based on X-ray structures (6.9 ppm) because of the exclusion of other important degrees of freedom, such as thiophene ring puckering.

The positions of the global minima as well as the dihedral angles from X-ray data are given in Table 5. Considering the 5° resolution in the calculated rotation, the agreement between modeling and X-ray is very good. Unfortunately, the sign of the dihedral angle cannot be reliably determined using this method. Since the input for these calculations required no knowledge of the X-ray data, the combination of molecular modeling and the experimentally derived local field tensors is a self-contained method for quantitatively determining structure not only in pharmaceutical polymorphs but also in any moderate-sized organic compounds.

TABLE 5: Comparison of the C11−C13−C16−S17 Dihedral Angles Derived from Molecular Modeling/Local Field Measurements and the X-ray Values

	$\theta_{\mathrm{C11-C13-C16-S17}}$ (deg)	
form	modeling	X-ray
ROY-R	41.0	43.6
ROY-O	58.0	50.1
ROY-Y	91.9	91.8

Conclusions

SSNMR can be a powerful method for studying structure in pharmaceutical solids. The sensitivity of interaction tensors to molecular conformation makes local field analysis of SSNMR line shapes an ideal tool for investigating conformation in polymorphic materials. The difficulty of utilizing SSNMR methods lies in the feasibility of extracting line shape information from the resulting spectra. Complicated line shapes, low sensitivity, poor resolution, and spectral crowding combined with the lack of tools necessary for distinguishing and identifying distinct molecular sites presents a large barrier to overcome before any useful information can be extracted from these spectra. A partial solution can be found by incorporating multidimensional SSNMR experiments, which provide effective means of increasing overall spectral resolution and facilitate measurements on moderate-sized organic molecules. In studies of local fields under MAS, the 2D PASS experiment is one of several very useful techniques for separating isotropic from anisotropic information over two-dimensions. The CSA tensor information encoded in the MAS manifolds can be used in conjunction with spectral editing experiments, spectral simulations of couplings to nearby (nitrogen) nuclear spins, and electronic structure calculations to assign isotropic resonances accurately, an important first step in any NMR structural study.

The aid of electronic structure calculations also makes it possible to extract structural information from measured chemical shift tensors. The ROY compounds provide a unique example of how chemical shifts change (nearly) exclusively with one molecular degree of freedom, namely, the phenyl−thiophene coplanar angle. This parametric dependence can be modeled using theoretical calculations and can yield quantitative information when compared with measured tensor values. The line shape analysis of the MAS manifolds for carbon sites coupled to quadrupolar nuclei yields direct measurements of carbon bond lengths and indirect structural information through the dipole and neighboring EFG tensors and their relative orientations. In situations where several sites are coupled to the same quadrupolar nucleus, the relative tensor orientations can be used to accurately determine bond angles. The principle values of the EFG tensor can be utilized in much the same way as the CSA tensor discussed above and can provide constraints to refine structure using theoretical calculations.

Though it may not be feasible to assign complete structures based solely on local field measurements, it should be possible to use this tensor information as constraints in a theory-based structure optimization process. With increasing computing power and speed, this process may well constitute a premier method for determining structure in solid materials.

Acknowledgment. The authors thank Eli Lilly and Company and Dr. Stephen Byrn for providing the samples used in these

experiments. Financial support from the National Institutes of Health and the National Science Foundation is gratefully acknowledged.

Supporting Information Available: Figures of 2D PASS pulse timings, experimental and theoretical CSA correlations, rotational potential energy surfaces, Mulliken charge analyses, and chemical shift calculations, as well as tables of experimental and calculated chemical shift tensor values, dipole/quadrupole orientation angles, and complete ref 34. This material is available free of charge via the Internet at http://pubs.acs.org.

References and Notes

(1) Byrn, S. R.; Pfeiffer, R. R.; Stowell, J. G. In *Solid-State Chemistry of Drugs*, 2nd ed.; SSCI, Inc.: West Lafayette, IN, 1999.

(2) He, X.; Griesser, U. J.; Stowell, J. G.; Borchardt, T. B.; Byrn, S. R. *J. Pharm. Sci.* **2001**, *90*, 371−388.

(3) Padden, B. E.; Zell, M. T.; Dong, Z.; Schroeder, S. A.; Grant, D. J. W.; Munson, E. J. *Anal. Chem.* **1999**, *71*, 3325−3331.

(4) Heller, J.; Laws, D. D.; Tomaselli, M.; King, D. S.; Wemmer, D. E.; Pines, A.; Havlin, R. H.; Oldfield, E. *J. Am. Chem. Soc.* **1997**, *119*, 7827−7831.

(5) Brender, J. R.; Taylor, D. M.; Ramamoorthy, A. *J. Am. Chem. Soc.* **2001**, *123*, 914−922.

(6) McMahon, M. T.; deDios, A. C.; Godbout, N.; Salzmann, R.; Laws, D. D.; Le, H. B.; Havlin, R. H.; Oldfield, E. *J. Am. Chem. Soc.* **1998**, *120*, 4784−4797.

(7) Mauri, F.; Pfrommer, B. G.; Louie, S. G. *Phys. Rev. Lett.* **1997**, *79*, 2340−2343.

(8) Potrzebowski, M. J.; Tekely, P.; Blaszczyk, J.; Wieczorek, M. W. *J. Pept. Res.* **2000**, *56*, 185−194.

(9) Stoltz, M.; Oliver, D. W.; Wessels, P. L.; Chalmers, A. A. *J. Pharm. Sci.* **1991**, *80*, 357−362.

(10) McGeorge, G.; Harris, R. K.; Chippendale, A. M.; Bullock, J. F. *J. Chem. Soc., Perkin Trans. 2* **1996**, *8*, 1733−1738.

(11) Dixon, W. T. *J. Chem. Phys.* **1982**, *77*, 1800−1809.

(12) Bax, A.; Szeverenyi, N. M.; Maciel, G. E. *J. Magn. Reson.* **1983**, *55*, 494−497.

(13) Terao, T.; Fujii, T.; Onodera, T.; Saika, A. *Chem. Phys. Lett.* **1984**, *107*, 145−148.

(14) Zeigler, R. C.; Wind, R. A.; Maciel, G. E. *J. Magn. Reson.* **1988**, *79*, 299−306.

(15) Tycko, R.; Dabbagh, G.; Mirau, P. A. *J. Magn. Reson.* **1989**, *85*, 265−274.

(16) Kolbert, A. C.; Griffin, R. G. *Chem. Phys. Lett.* **1990**, *166*, 87−91.

(17) Gan, Z. *J. Am. Chem. Soc.* **1992**, *114*, 8307−8309.

(18) Frydman, L.; Chingas, G. C.; Young, K. L.; Grandinetti, P. J.; Eastman, M. A.; Barrall, G. A.; Pines, A. *J. Chem. Phys.* **1992**, *97*, 4800−4808.

(19) Feaux de Lacroix, S.; Titman, J. J.; Hagemeyer, A.; Spiess, H. W. *J. Magn. Reson.* **1992**, *97*, 435−443.

(20) Antzutkin, O. N.; Shekar, S. C.; Levitt, M. H. *J. Magn. Reson., Ser. A* **1995**, *115*, 7−19.

(21) Alderman, D. W., McGeorge, G.; Hu, J. Z.; Pugmire, R. J.; Grant, D. M. *Mol. Phys.* **1998**, *95*, 1113−1126.

(22) Strohmeier, M.; Grant, D. M. *J. Magn. Reson.* **2004**, *168*, 296−306.

(23) Antzutkin, O. N.; Lee, Y. K.; Levitt, M. H. *J. Magn. Reson.* **1998**, *135*, 144−155.

(24) Barich, D. H.; Clawson, J. S.; Stueber, D.; Strohmeier, M.; Pugmire, R. J.; Grant, D. M. *J. Phys. Chem. A* **2002**, *106*, 11375−11379.

(25) Strohmeier, M.; Grant, D. M. *J. Am. Chem. Soc.* **2004**, *126*, 966−977.

(26) Smith, J.; MacNamara, E.; Raftery, D.; Borchardt, T.; Byrn, S. *J. Am. Chem. Soc.* **1998**, *120*, 11710−11713.

(27) Harper, J. K.; Grant, D. M. *J. Am. Chem. Soc.* **2000**, *122*, 3708−3714.

(28) Barich, D. H.; Pugmire, R. J.; Grant, D. M.; Iuliucci, R. J. *J. Chem. Phys. A* **2001**, *105*, 6780−6784.

(29) Stephenson, G. A.; Borchardt, T. B.; Byrn, S. R.; Bowyer, J.; Bunnell, C. A.; Snorek, S. V.; Yu, L. *J. Pharm. Sci.* **1995**, *84*, 1385−1386.

(30) de Groot, H. J. M.; Smith, S. O.; Kolbert, A. C.; Courtin, J. M. L.; Winkel, C.; Lugtenburg, J.; Herzfeld, J.; Griffin, R. G. *J. Magn. Reson.* **1991**, *91*, 30−38.

(31) Suits, B. H.; Sepa, J.; White, D. *J. Magn. Reson.* **1996**, *120*, 88−96.

(32) Alderman, D. W.; Solum, M. S.; Grant, D. M. *J. Chem. Phys.* **1986**, *84*, 3717−3725.

(33) Press, W. H.; Teukolsky, S. A.; Vetterling, W. T.; Flannery, B. P. *Numerical Recipes in C*$^{++}$. *The Art of Scientific Computing*, 2nd ed.; Cambridge University Press: New York, 1992; pp 408−412.

(34) Frisch, M. J.; et al. *Gaussian 98*, revision A.7; Gaussian, Inc.: Pittsburgh, PA, 1998.

(35) Becke, A. D. *J. Chem. Phys.* **1993**, *98*, 5648−5652.

(36) Lee, C.; Yang, W.; Parr, R. G. *Phys. Rev. B* **1988**, *37*, 785−789.

(37) McLean, A. D.; Chandler, G. S. *J. Chem. Phys.* **1980**, *72*, 5639−5648.

(38) Krishnan, R.; Binkley, J. S.; Seeger, R.; Pople, J. A. *J. Chem. Phys.* **1980**, *72*, 650−654.

(39) Ditchfield, R. *Mol. Phys.* **1974**, *27*, 789−807.

(40) Strohmeier, M.; Orendt, A. M.; Alderman, D. W.; Grant, D. M. *J. Am. Chem. Soc.* **2001**, *123*, 1713−1722.

(41) Poon, A.; Birn, J.; Ramamoorthy, A. *J. Phys. Chem. B* **2004**, *108*, 16577−16585.

(42) Yu, L.; Stephenson, G. A.; Mitchell, C. A.; Bunnell, C. A.; Snorek, S. V.; Bowyer, J. J.; Borchardt, T. B.; Stowell, J. G.; Byrn, S. R. *J. Am. Chem. Soc.* **2000**, *122*, 585−591.

(43) Opella, S. J.; Frey, M. H.; Cross, T. A. *J. Am. Chem. Soc.* **1979**, *101*, 5856−5857.

(44) Olivieri, A. C. *J. Magn. Reson. A* **1993**, *101*, 313−316.

(45) Hallock, K. J.; Lee, D. K.; Ramamoorthy, A. *J. Chem. Phys.* **2000**, *113*, 11187−11193.

(46) Liboff, R. L. *Introductory Quantum Mechanics*, 2nd ed.; Addison-Wesley Publishing: Reading, MA, 1992; p 201.